Influence of alternative fuel properties and combustor operating conditions on the nvPM and gaseous emissions produced by a small-scale RQL combustor

Joseph Harper [a*], Eliot Durand [a*], Andrew Crayford [a], Mark Johnson [b], Daniel Pugh [a], Philip Bowen [a]

[a] Gas Turbine Research Centre, Cardiff University, Cardiff, United Kingdom

[b] Rolls-Royce, plc., Sin A-37 PO Box 31, Derby, UK, DE24 8BJ

[*] Corresponding authors
E-mail address: harperj4@cardiff.ac.uk, DurandEF@cardiff.ac.uk
Postal address: Cardiff School of Engineering, Queen's buildings, 14-17 The Parade, Cardiff, CF24 3AA, United Kingdom

1. Introduction

Civil aviation gas turbine engines are known to emit numerous harmful pollutants which negatively impact both the local and global environment, including Carbon Dioxide (CO_2), Nitrous Oxides (NOx), Carbon Monoxide (CO) and Unburned HydroCarbons (UHCs) [1]. Alongside gaseous emissions, aircraft engines emit ultrafine non-volatile Particulate Matter (nvPM) with diameters typically less than 100 nm [2–6]. These emissions are formed in localised areas of poor fuel-air mixing and incomplete combustion in the primary zones of combustors [7,8] and have been linked to serious degradation of Local Air Quality (LAQ) near airports [9,10], as well as increased rates of lung cancers and cardiovascular/respiratory diseases [11]. In 2015, it was estimated that global $PM_{2.5}$ emissions (<2.5µm particle diameter) from commercial aircraft were responsible for almost 14,000 premature deaths per annum [12], a statistic expected to worsen with the predicted growth in air travel. It has also been shown that nvPM exhibits regional warming effects both when airborne and when deposited on polar ice/snow, while aircraft nvPM presents the unique issue of acting as condensation sites for cirrus cloud contrail formation at high altitudes, contributing to global radiative forcing [1,13–15]. The contribution of cloud cirrus contrails to effective radiative forcing from aviation is believed to be similar or greater even than that of CO_2 [1,15,16]. In response to the above issues, the International Civil Aviation Organization (ICAO) introduced in 2020 regulations concerning nvPM emissions from gas turbine engines with a rated thrust >26.7kN [17].

Approaches to mitigating aircraft emissions include developments in both combustor technologies and alternative aviation fuels. Engine manufacturers strive for continual improvements in performance, with an aspirational goal of 2% p.a. improvement to fuel burn per passenger km outlined by ICAO [18]. Alternative low-emission combustor technologies including Rich-Quench-Lean (RQL) and Lean-burn technologies are currently used and being further developed. RQL combustors are low-NOx technologies which have been successfully applied to Rolls-Royce Trent, GE CMF56 and Pratt & Whitney PW6000 engines as part of the TALON combustor family [19]. These combustors utilise fuel rich primary zones with large volumes of dilution air to minimise the residence time of the combustion

process near stoichiometry and achieve low NOx emissions, but are known to be susceptible to increased PM and CO formation in their primary zones [8]. However, improvements to combustor technologies are only capable of emissions reduction to a certain extent hence are not expected to mitigate the expected rise in carbon emissions from international aviation on their own [18].

Because fuels refined from crude oil invariably produce harmful emissions (especially CO_2) during combustion, alternative fuel sources are a key area of development in the mitigation of emissions. The most widely used fuels in modern commercial aviation are Jet-A1 (Europe) and Jet A (US), both refined from crude oil and regulated by the ASTM D1655 standard [20]. These fuels may contain up to 25% aromatic content (% vol), which generally exhibit reduced specific energies compared to paraffinic components [21], and are widely agreed to be the primary cause of nvPM formation in combustion engines [8,22,23]. The adoption of alternative fuels with low aromatic contents is therefore a promising solution to nvPM emissions from aircraft. In particular, alternative fuels conforming to the "drop-in" concept i.e. requiring minimal or zero modification to existing aircraft designs for use, could act as a near term bridge between existing conventional fuels and longer term alternative fuel sources such as liquid hydrogen [24,25]. Synthetic liquid fuels manufactured from sustainable biological feedstocks capable of significant carbon capture [21] or from renewable energy sources via. Power-to-Liquid conversion [26] may be classified as Sustainable Aviation Fuels (SAF), which are key developments towards a carbon neutral aviation sector. At the time of writing, eight SAF conversion processes are approved for use in aviation [27,28] although optimisation issues with the use of neat SAF in existing aircraft, including poor O-ring seal swell behaviour leading to fuel tank leakage for fuels below a certain aromatic threshold (<8% vol. [29]), mean SAF are currently only suitable as blends with conventional fuels up to maximum volume limits prescribed by the ASTM D7566 document [27].

Previous studies have observed significant achievable reductions in nvPM emissions by the use of low aromatic drop-in fuels and SAF in gas turbine engines [30–35]. Recently, low aromatic SAF blends were shown to reduce cloud contrail formation and lessen radiative forcing [36]. Total aromatic content often shows strong correlations with nvPM emissions due to the key role of aromatics in nvPM

formation, and can be used alone as a “first order” parameter in simple empirical predictions [37]. However, attributing soot formation to total aromatic content alone ignores sooting tendencies across aliphatic hydrocarbons or different types of aromatic compounds. Straight chained and branched paraffins are thought to form PM through slower pyrolytic fragmentation and growth reactions [38–41], while cycloparaffins are responsible for a greater degree of PM than paraffins, though less than aromatic compounds [30,42]. Historically, a hierarchy of sooting tendencies across hydrocarbon families was established by Calcote and Manos [43] as follows; *paraffins* < *iso-paraffins* < *cyclo-paraffins* < *mono-aromatics* < *di-aromatics (naphthalenes)* < *poly-aromatics.* This is better represented by fuel hydrogen content (or H/C ratio), which is currently used as the first order parameter best describing nvPM formation [34,44]. Despite this however, it has been suggested that hydrogen content used on its own is insufficient in fully describing nvPM emissions, since both chemical and physical properties may affect nvPM formation [42,45,46]. Physical properties such as surface tension, kinematic and dynamic viscosity, and density can impact gas turbine combustion by affecting atomisation quality and fuel/air mixing prior to combustion, where improved atomisation quality (i.e., smaller droplets) and even mixing reduces nvPM formation in a gas turbine [7,47]. Although the effects of these properties may be small enough compared to chemical influences to not have warranted consideration in prior alternative fuel studies, the typical variability encountered when considering drop-in fuels (5-10%) makes them relevant nevertheless [48].

Categorising all the effects of fuel properties on nvPM formation proves difficult in aircraft engine tests since the flow processes are complex. Modern computational modelling of flow behaviours, combustion chemistry and emissions formation provides improved understanding of experimentally observed combustion behaviour in gas turbines [49,50]. However, accurately capturing the complex nature of real-world gas turbines and soot formation chemistry remains challenging and computationally intensive given the many components (often varying between batches) of real-world Jet-A1 fuels. Therefore, modelling studies have been limited to using single-component fuels to capture physical or chemical general trends [47], or surrogate fuels containing a select few components chosen to replicate key physiochemical properties of a target fuel [51–54]. Recently, the field of chemical modelling has

specialised for jet fuel combustion, towards higher accuracy nvPM formation at reduced computational cost [49,55–57]. Novel modelling techniques and dedicated kinetic models based on experimental data continue to be developed for conventional and alternative fuels [56,58]. To validate modelling studies of this nature, accurate and comprehensive experimental data is essential, but remains limited for aero-engine combustors under well-defined conditions [57]. This is especially complicated as regulation of aircraft nvPM emissions prescribes a long sampling system (up to 35 m line length) which results in particle loss as high as 90% for nvPM number concentration and up to 50% for nvPM mass concentration [59]. Particle losses are greater when particle sizes are smaller, as is typical of low-aromatic bio-fuels compared to conventional fuels [38], which can lead to an overprediction of achievable emissions reductions unless corrected for. To allow for accurate characterisation of fuel and combustor effects, it is therefore necessary to correct for particle loss in the sampling system [3,34].

In this study a small-scale (<250kW) non-proprietary, Cardiff University Gas Turbine Research Centre (GTRC) RQL combustor, was operated as part of the H2020 JETSCREEN (JET fuel SCREENing and optimisation platform for alternative fuels) project. Full ICAO regulatory compliant nvPM and gaseous emissions data were obtained, using the European (EUR) nvPM reference system, for nine aviation fuels (conventional, SAF and blended) over a range of combustor operating conditions and pressures. Measured concentrations of nvPM were corrected for system losses, to be representative of the emissions at the combustor exit, which are presented with full details of the geometries, flow conditions and rig conditions of the RQL combustor, affording insight into the impact of fuel and operating conditions on nvPM formation and thus providing a unique dataset for validation of combustion emission models.

2. Material and methods

2.1. Fuels

Nine fuels were investigated with a summary of their physiochemical properties presented in **Table 1** and **Figure 1**. The fuels include three conventional aviation Jet-A1 fuels (J-REF, J-LA, and J-HA), three SAF's of various manufacturing origins (A-LA, A-MA, and A-HA) and three blends (B-

REF, B-HE1 and B-HE2). Four of these fuels have been tested previously during the ECLIF II Campaign to study the impact of SAF on cloud contrail formation [36]. Fuel hydrogen content was measured from fuel samples following the ASTM D7171 standard [60]. Detailed fuel compositional analysis was undertaken using 2-Dimensional Gas Chromatography (GCxGC) for all fuels except A-MA, whose compositional properties had already been determined using various ASTM methods. Hydrogen content values calculated separately from GCxGC data agreed well with values determined from ASTM D7171 [60], with no more than 0.243% difference between the two. In this study mono-aromatic compounds are classified as any molecule containing a benzene ring, including those with branched and naphthenic functional groups, while di-aromatics are classified similarly for molecules containing two benzene rings. The polyaromatic content (i.e., aromatic compounds containing three benzene rings and above) was negligible across all fuels.

Fuel kinematic viscosity, surface tension and density measured values were taken to afford an insight into expected atomisation behaviour across fuels. Viscosity measurements were undertaken using an Otswald BS/U-tube viscometer for clear liquids (±0.22%) at a fuel preheat temperature of 25°C. Surface tension measurements were undertaken using a KRUSS K10T tensiometer fitted with a platinum du noüy ring (±0.05 mN/m). Liquid density at 15°C was measured using a Bronkhorst mini-CORI-FLOW M14 Coriolis mass flow controller, except for fuel A-MA, which density had been predetermined using the IP 365 oscillating U-tube method for petroleum fuels. Dynamic viscosities were calculated from measured kinematic viscosity and density values.

The conventional aviation fuels (i.e., J-REF, J-LA and J-HA) all conformed to the ASTM D1655 standard [20] but had different compositions and physical properties. A typical Jet-A1 fuel (14.022% hydrogen content) acted as the reference fuel in this study. J-HA was a high aromatic (low hydrogen content) Jet-A1 with a reduced sulphur content, while J-LA was a de-sulphurised Jet-A1 with similar monoaromatic content to J-REF but a low di-aromatics content. The SAF consisted of two Alcohol-to-Jet (ATJ) fuels: one ATJ-SPK composed of almost entirely iso-paraffins with low aromatic content (A-

LA), the other a Byogy fully formulated ATJ containing a moderate quantity of aromatic compounds (A-MA). Fuel A-MA was found to possess a relatively higher kinematic viscosity which is suggested may be a function of fuel aging. The third SAF (A-HA) was a Catalytic Hydrothermal Conversion Jet (CHCJ) fuel with the highest total aromatic content in the study (consisting of almost entirely mono-aromatics). All the SAF fuels possessed higher viscosities than the conventional aviation fuels and blends irrespective of hydrogen and total aromatic content. Finally, three blends were formulated of conventional and SAF fuels, mixed to fall within the limits defined by ASTM D7566 [27]. B-REF was a mixture of 70% J-REF with 30% A-LA by volume. The other two blended fuels (B-HE1 and B-HE2) contained a highly paraffinic HEFA fuel with negligible aromatic content. Fuel B-HE1 consisted of 51% J-HA with 49% HEFA by volume, while fuel B-HE2 had a similar total aromatic content but lower di-aromatic content and consisted of 70% J-LA with 30% HEFA. Fuel J-LA (and subsequently B-HE2) exhibited a comparably low viscosity. Across all fuels studied, measured densities showed well defined inverse correlations with hydrogen content.

Fuel	**A-HA**	**J-HA**	**J-REF**	**J-LA**	**B-HE1**	**B-REF**	**A-MA**	**B-HE2**	**A-LA**
Hydrogen Content (%wt) (ASTM D7171)	**13.510** (±0.007)	**13.649** (±0.046)	**14.022** (±0.024)	**14.083** (±0.029)	**14.397** (±0.074)	**14.405** (±0.006)	**14.422** (±0.004)	**14.514** (±0.036)	**15.310** (±0.003)
Specific Energy (MJ/kg) (ASTM D4809/ASTM 3338)	**43.302**	**42.851**	**43.355**	**43.049**	**43.37**	**43.62**	**43.61**	**43.326**	**44.159**
GCxGC Mono-Aromatics (%wt)	**24.91**	**20.57**	**18.41**	**17.82**	**11.48**	**12.89**	**11.4**	**12.68**	**0**
GCxGC Di-Aromatics (%wt)	**0.28**	**2.18**	**1.82**	**0.18**	**1.22**	**1.28**	**0.1**	**0.14**	**0**
GCxGC Total Aromatics (%wt)	**25.18**	**22.75**	**20.24**	**18.01**	**12.7**	**14.16**	**11.5**	**12.82**	**0**
Sulphur (ppm) (ASTM D2622)	**0**	**105**	**200**	**5.7**	**56.8**	**140**	**0**	**4.1**	**0**
Kinematic Viscosity 25^{o}C (mm2/s)	**1.72**	**1.62**	**1.62**	**1.3**	**1.59**	**1.64**	**2.09**	**1.39**	**1.74**
Surface Tension 25^{o}C (mN/m)	**27.6**	**27**	**25.9**	**25.67**	**25.63**	**25.07**	**25.8**	**25.23**	**27**
Density 15^{o}C (kg/m3)	**828**	**817**	**798**	**793**	**789**	**790**	**791**	**782**	**768**

Table 1: Summary of the physiochemical properties for the nine investigated fuels

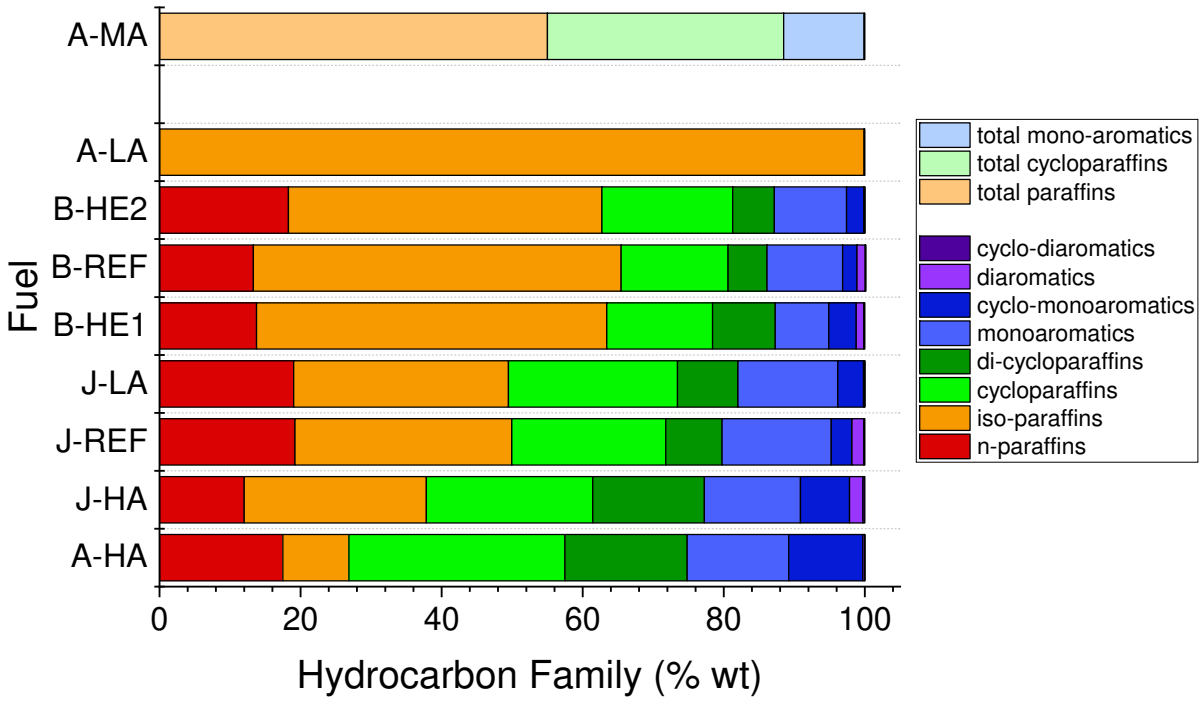

Figure 1: Clustered column graph displaying the chemical compositions of the investigated fuels

2.2. RQL Combustor Design

The combustor developed for this study (Figure 2) was a scaled 250kW, 85mm internal diameter, fixed geometry RQL combustor based on the concepts proposed by Makida et al. [61]. The scaled setup allowed for the investigation of nvPM and gaseous emissions while requiring a relatively lower amount of fuel compared to full-scale GT testing. Fuel was delivered using a pre-filming airblast atomiser following a Parker-Hannifin design [62]. The atomiser, shown in

Figure 2, was manufactured from 316L stainless steel using a Powder Bed Fusion (PBF) laser additive manufacturing process as a further iteration of the design discussed in Crayford et al. [63]. The design of the atomiser consists of an inner and outer air channel surrounding a middle fuel channel. The counter-rotating air streams contain internal blades (45° inner and 60° outer) applying swirl, while the fuel channel swirler (45°) co-rotates with the inner air, promoting the development of a uniform liquid sheet and ensuring optimal atomisation performance [64]. The film thickness of the fuel was calculated by difference of diameters and found to be 0.43mm for this design. Geometric swirl numbers were calculated as 0.848 for the inner air channel, 0.942 for the fuel channel and 1.448 for the outer air channel, indicative of a strongly swirling flow [65].

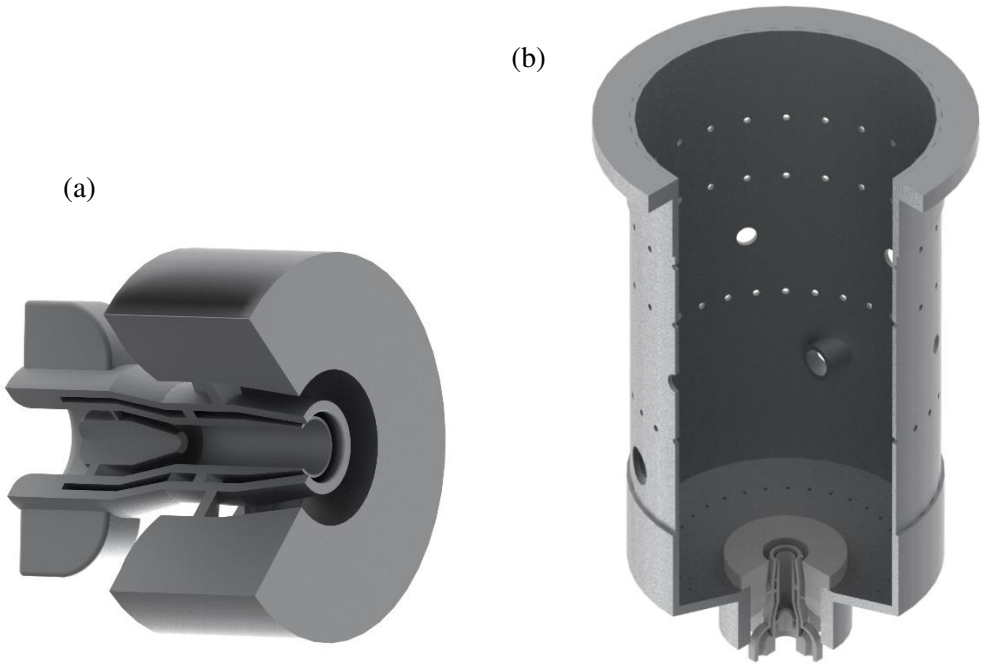

Figure 2: ALM airblast atomiser design (left) and RQL combustor liner with atomiser placement (right)

The RQL combustor was housed within a High-Pressure Operating Chamber (HPOC) as shown in **Figure 3**, capable of affording elevated combustor pressures (1-16 bara). Primary and secondary air flows dried to a fixed dew point of -17°C using a Beko Drypoint RA DPRA960 were supplied from two Atlas Copco GA45VSD variable speed drive compressors and independently regulated using an Emerson CMF025M and CMF050M (±0.35%), respectively. Fuel supply was regulated using a Bronkhorst mini-CORI-FLOW M14 Coriolis mass flow controller (±0.2%). Fuel and primary air, nominally preheated to 30ºC and 80ºC respectively, were supplied to the atomiser via a fuel/air lance, while secondary air was preheated to nominally 120°C and supplied into the HPOC before entering the combustor liner. The preheating of each fluid flow was intended to eliminate uncertainties associated with flow behaviours or fuel physical properties caused by day-to-day variability of ambient temperature. K-type thermocouples were positioned in various locations of the experimental setup to monitor temperatures during operation, recorded by the centralised data logging system at 1 Hz capture rate. Static pressure taps were located on the primary air inlet line, in the HPOC casing and in the front

face of the combustor liner, allowing pressure drop values across the atomiser and combustor liner to be determined.

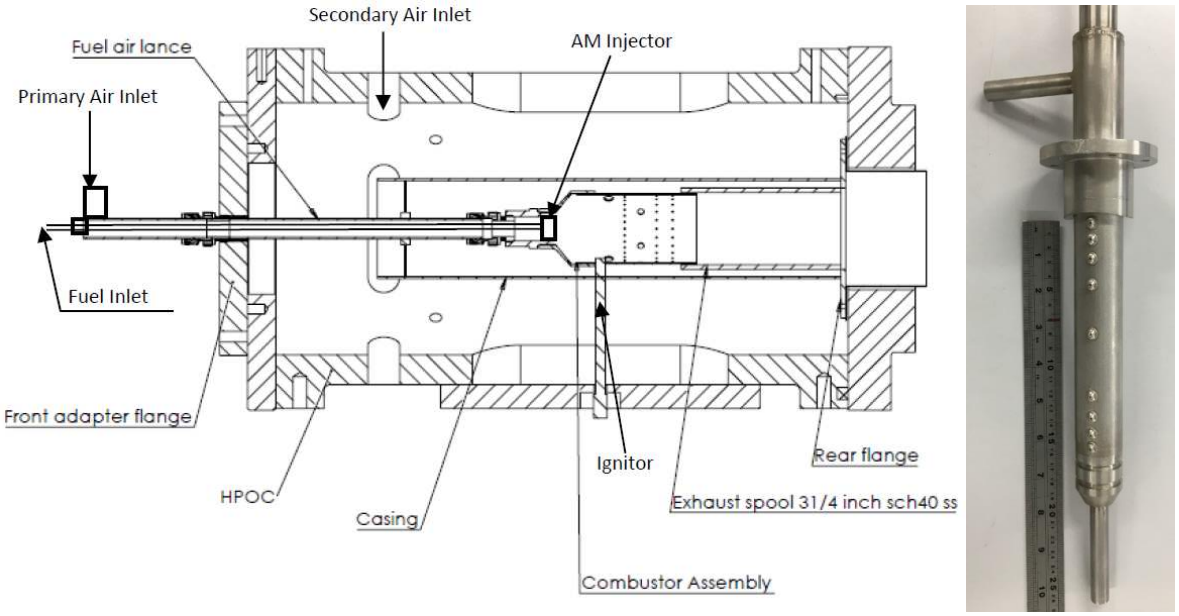

Figure 3: Diagram of the RQL combustion rig (left) and Piccolo sampling probe (right)

2.3. Test matrix

Over the course of the experimental programme, measurements were taken on fourteen stable (as defined in section **3.1**) test points across four combustor pressures for each fuel, as shown in

. Flowrates and preheat temperatures were chosen so as to maintain individual pressure drops across the atomiser and combustor at levels suitable for aircraft engines (3-4% [8]). However, it should be noted that these operating conditions are not representative of in-service engine operating conditions, being lower in power and pressure, and were instead chosen to allow for long run times needed to generate a comprehensive dataset with the available fuels, whilst also protecting the liner from thermal damage. Global ERs of 0.30-0.37 and primary zone ER's (including primary cooling air) of 2.91-3.67 were calculated. This high primary zone equivalence ratio ensured sufficient nvPM formation hence allowing fuel effects to be investigated. The combustor rig and nvPM measuring equipment were cleaned daily to remove any soot deposits formed during each test from the combustor can wall or within the exhaust sections prior to sample probe. As pressure conditions increased, flow conditions

were scaled on a 32kW/bar drive-line. A total of 126 discrete data-points were taken with no repeats afforded due to time constraints and limited fuel supply.

Combustor Pressure (bara ±3.9%]	Condition	Fuel Mass Flowrate (g/s ±0.4%)	Primary Air Mass Flowrate (g/s ±2.0%)	Secondary Air Mass Flowrate (g/s ±0.4%)	Primary Equivalence Ratio (±1.3%)	Global Equivalence Ratio (±0.4%)
1.03	**A**	**0.71**	**2.10**	**30.02**	**3.20**	**0.33**
1.03	**B**	**0.71**	**2.42**	**30.02**	**2.91**	**0.33**
1.03	**C**	**0.81**	**2.09**	**30.01**	**3.66**	**0.37**
1.03	**D**	**0.81**	**2.42**	**30.01**	**3.33**	**0.37**
1.44	**C**	**1.21**	**3.12**	**44.98**	**3.67**	**0.36**
1.41	**D**	**1.21**	**3.62**	**45.00**	**3.32**	**0.36**
1.92	**A**	**1.41**	**4.18**	**60.00**	**3.20**	**0.31**
1.89	**B**	**1.41**	**4.81**	**60.02**	**2.91**	**0.31**
1.93	**C**	**1.61**	**4.19**	**60.13**	**3.65**	**0.35**
1.86	**D**	**1.61**	**4.81**	**60.01**	**3.33**	**0.35**
1.93	**E**	**1.61**	**4.19**	**70.12**	**3.44**	**0.31**
2.41	**C**	**2.01**	**5.25**	**74.96**	**3.64**	**0.34**
2.37	**D**	**2.01**	**6.02**	**75.08**	**3.32**	**0.34**
2.41	**E**	**2.01**	**5.23**	**87.57**	**3.44**	**0.30**

Table 2: RQL Combustor rig operating conditions (± max % variability across fuels)

2.4. Particulate and gaseous sampling and measurement

A representative sample of the RQL combustor exhaust was extracted using a water cooled (433K) 9-point equal area 'piccolo' sampling probe with sampling orifices 1.2 mm diameter, located approximately 400mm from the combustor outlet. The probe was housed in a water-cooled exhaust duct, which was approximately 170 mm diameter. The exhaust was then further conditioned in a water-cooled (433K) heat exchanger (1 m long 3/8'' ID) before being split between the dedicated gaseous measurement system and the EUR reference nvPM sampling and measurement system, which is further detailed elsewhere [34,66]. The exhaust aerosol was transferred to the EUR nvPM system via a 2 m

long, 8 mm ID, anti-static (carbon loaded) polytetrafluoroethylene (PTFE) sample line heated at 433K. In line with Appendix 7 of ICAO Annex 16 Vol. II [67], the nvPM sample was diluted and cooled to 333K, suppressing the potential for particle coagulation, water condensation, and volatile particle nucleation with the dilution factor confirmed as compliant (8-14) using CO_2 measurement (Rosemount NGA MLT). The diluted aerosol was then transported via a 25 m long, 8 mm ID, 333K, anti-static PTFE sample line, to a 1 µm sharp-cut cyclone before measurement. The nvPM number concentrations were attained using an AVL Advanced Particle Counter (APC) which consists of a two-stage diluter with an integral catalytic stripper and a TSI 3790E Condensation Particle Counter (CPC). The nvPM mass concentrations reported were measured using an AVL Micro Soot Sensor (MSS). Additional mobility-space particle size measurement was performed using a suitably calibrated (aggregate inversion matrix) Cambustion fast-mobility spectrometer (DMS-500) which, as discussed later, provided loss correction.

Parallel gaseous measurements of NOx, UHC and CO were performed using calibrated heated vacuum chemiluminescence (Signal Instruments 4000VM), flame ionisation detector (Signal Instruments 3000HM) and nondispersive infrared (Signal instruments 9000MGA) analysers, respectively.

3. Calculations

3.1. Data processing

The nvPM and gaseous emissions data presented in this study correspond to a 30-second average of 1 Hz data collected at a stable condition (30-second average coefficient of variation of 2.7±2.3% for nvPM number, 5.8±3.5% for nvPM mass, and <0.1% for raw CO_2). The nvPM number and mass emissions are reported as Emission Indices (EIs) and are corrected to the combustor exit location. The EI metric expresses emissions per unit mass of fuel burned rather than per volume of exhaust air, and were calculated using the simplified method as defined in the relevant aerospace practice SAE ARP 6320 [68]. Combustor-exit nvPM number and mass EIs were calculated from the measured EIs by correcting for particle losses in the system using equation (1).

$$\mathbf{EI_{nvPM\ EEP}} = \mathbf{EI_{meas}} \times \boldsymbol{k}_{\mathbf{SL}} \times \boldsymbol{k}_{\mathbf{thermo}} \quad (1)$$

where EI_{meas} is the measured simplified nvPM EI, k_{thermo} is the thermophoretic loss correction factor in the collection section of the sampling system, and k_{SL} is the size-dependent system loss correction factor calculated using the UTRC model and measured particle size distribution (i.e. bin by bin particle loss correction) rather than the standard ARP6481 method [59], as has been used elsewhere [34].

NOx, CO and UHC emissions are also reported as EIs given they relate engine performance and environmental impact. Gaseous EIs underwent a correction process specified in the SAE ARP 1533 for gaseous measurements [69] to account for water vapour, O_2 broadening, interference and conversion efficiency of the NOx analyser.

3.2. Predicted Impact of Fuel Physical Properties on Spray Quality

Fuel atomisation quality of the developed atomiser was assessed empirically using water spray tests. Values of Sauter Mean Diameter (SMD), commonly used to represent atomisation quality in combustion applications [70] were measured using a Malvern Spraytech97 particle sizer, at atomisation air preheat temperatures of ~80°C, with air flowrates ranging from 2 – 10 g/s and a fixed water flowrate of 0.8 g/s under atmospheric pressures. Measurements were taken at a point 40mm downstream of the atomiser exit, equal to the primary air hole locations. The standard deviations for the data points were computed by the Malvern operating software. As observed in **Figure 4 (a)**, the measured values of SMD produced by the atomiser correlated well with predicted values using an empirical airblast atomiser correlation proposed by El-Shanawany and Lefebvre [71] (**equation (2)**).

$$SMD = 0.073\left(\frac{\sigma}{\rho_a U_R^2}\right)^{0.6}\left(\frac{\rho_L}{\rho_a}\right)^{0.1} {D_p}^{0.4}\left(1+\frac{1}{ALR}\right) + 0.015\left(\frac{\mu_L^2 D_p}{\sigma\rho_L}\right)^{0.5}\left(1+\frac{1}{ALR}\right) \quad (2)$$

Where ρ_a and ρ_L are densities of the air and fuel respectively, σ is fuel surface tension, μ is fuel dynamic viscosity and ALR is the air/fuel ratio. Pre-filming diameter (D_p) was equated to the inner fuel channel wall against which the liquid sheet is formed (5.5 mm) and the relative velocity (U_r) of the air

to fuel was calculated using Bernoulli's equation and total exit orifice area of both air channels. After benchmarking **equation (1)** using water (σ=72.8 mN/m, μ=1.001 mPa.s, ρ=998 kg/m^3) and air as the atomising fluids, the relevant experimental and fuel parameters from the RQL tests were used to predict the SMDs corresponding to the experimental conditions chosen for this study. An example dataset for the nine fuels at a given condition are presented in **Figure 4 (b)**.

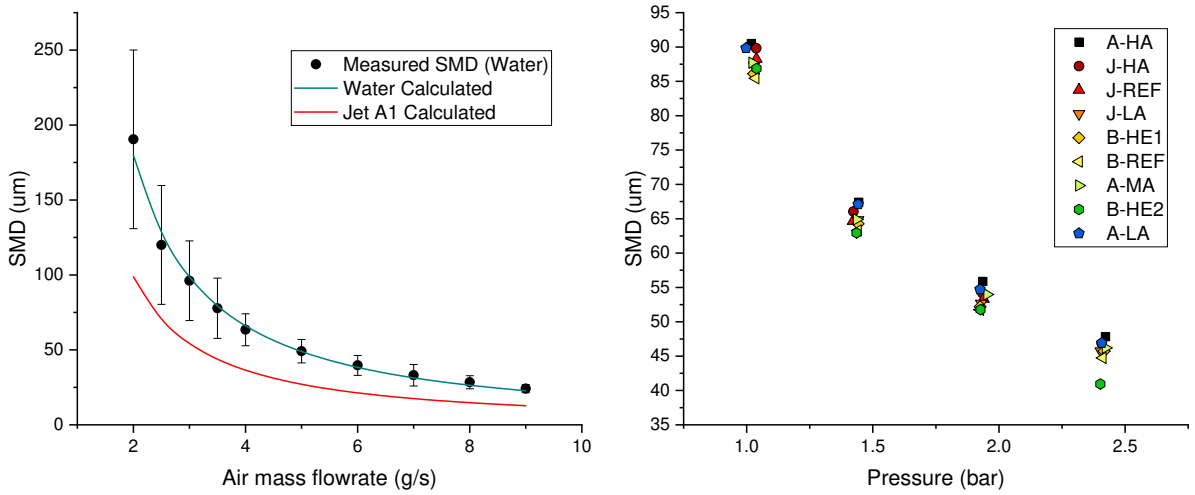

Figure 4: Measured and predicted SMD from the nozzle when atomising 0.8 g/s of water (a) and Predicted SMD for different fuels and combustor pressures at combustor rig condition C (b)

Figure 4 (b) highlights that spray quality is predicted to vary because of both fuel physical properties and rig conditions, with maximum variations in predicted SMD across fuels of approx. 7 μm (15.6%) observed at the 2.4bar condition. A-HA is generally predicted to produce the coarsest sprays (largest SMD) while B-REF produced the finest (smallest SMD). As discussed, primary air mass flowrates were scaled with pressure ensuring primary velocities and AFR remained constant, but air density increased with pressure, which explains the improved atomisation predicted at ~90 μm at 1 bar down to ~45 μm at 2.4 bar. For comparison, SMD values in Gas Turbines typically fall between 40-80 μm [72]. Assuming the fuel is incompressible, the increase in fuel flowrate at higher pressure conditions would be expected to slightly increase SMD values due to a reduction in relative velocity between the air and fuel (U_R) and subsequent increase in Weber number (We), but would have no effect on primary AFR.

4. Experimental Results and Discussion

4.1. nvPM Emissions

nvPM emissions as measured and reported in compliance with ICAO Annex 16 Vol II [67] ranged from 1.8 to 364.2 mg/kg fuel for EI_{mass} and 6.41E+13 to 1.98E+15 particles/kg fuel for EI_{number}, corresponding to a similar order of magnitude reported in the literature for full-scale aircraft gas turbine engines [2,4–6,73]. Measured Particle Size Distributions (PSD) were also in agreement with the published literature [3,74], being monomodal in shape with Geometric Mean Diameters (GMDs) ranging from 26.6-53.3 nm and with Geometric Standard Deviations (GSD) between 1.74-1.93. GMD was seen to generally increase with decreasing hydrogen content (see example PSDs at 2.4 bar combustor pressure at rig operating condition C in **Figure 5**) and increasing combustor rig pressure (see section **4.1.1**). As discussed in section **3.1**, particle size distributions measured at the end of the European reference sampling and measurement system were subsequently used to predict the size-dependent particle losses required to calculate the nvPM EIs emitted at the combustor exit.

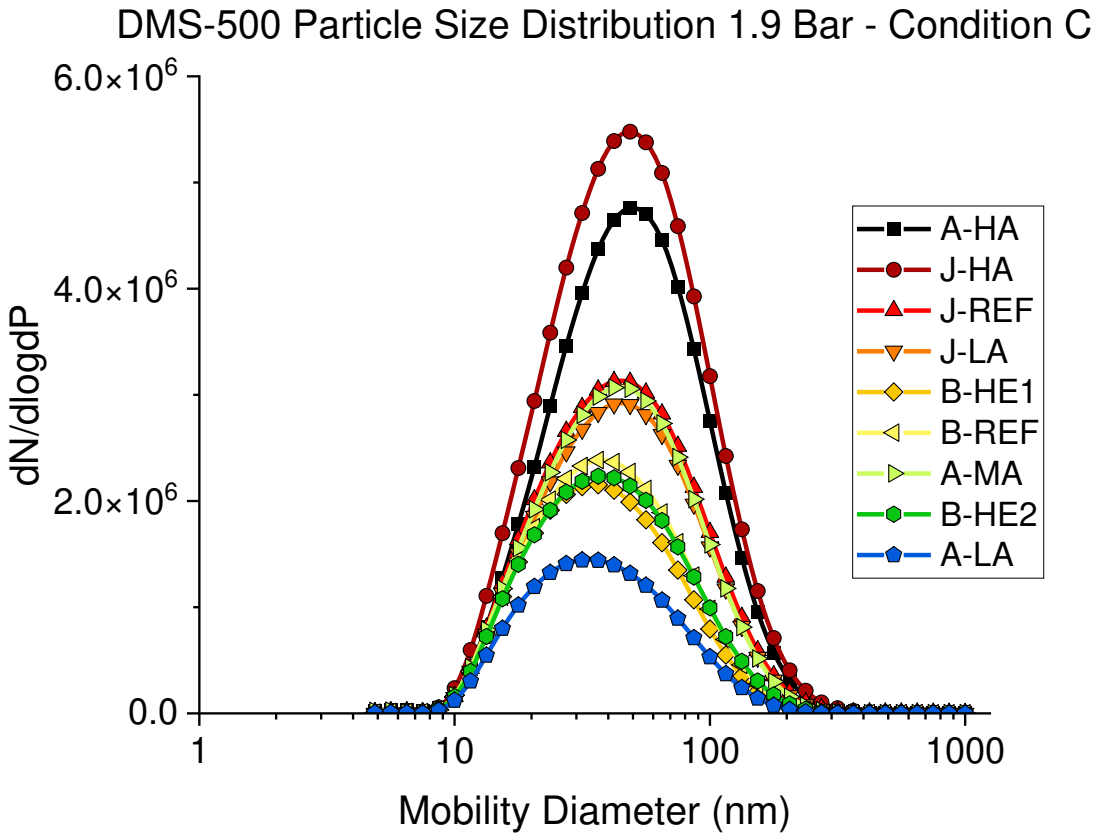

Figure 5: Particle size distribution measured by DMS-500 for the nine fuels at 1.9 bar combustor pressure and rig operating condition C (legend top to bottom – decreasing fuel hydrogen content)

4.1.1. Impact of fuel hydrogen content and combustor pressure on nvPM emissions

The effects of varying the fuel hydrogen content from 13.51 to 15.31% and increasing combustor pressure from 1 to 2.4 bar on combustor-exit corrected nvPM EI_{mass}, EI_{number} and Engine Exit Plane (EEP) corrected GMD are displayed in **Figure 6**. Corrected values of EI_{mass} and EI_{number} ranged between 2.1 to 396.8 mg/kg fuel and 2.31E+14 to 4.34E+15 particles/kg, respectively. Combustor-exit GMD values ranged from 20.5 to 43.6nm, as expected from the higher number of smaller particles measured reducing the mean diameter. Inverse power fits are added for visual aid with error bars representing ±2 standard deviations of a 30-second average at a nominally stable operating condition.

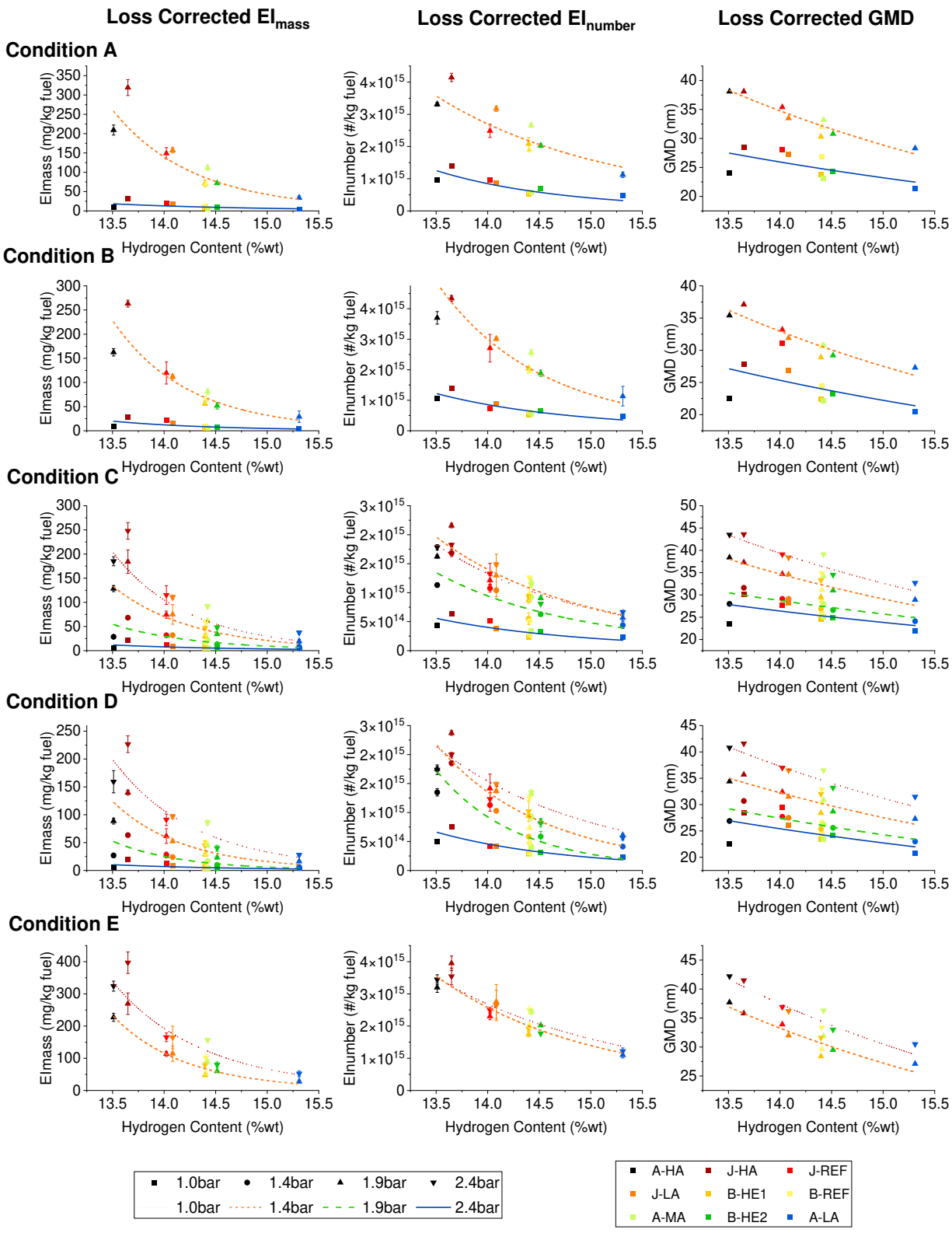

Figure 6: Combustor-exit nvPM EI$_{mass}$, EI$_{number}$ and EEP GMD against fuel hydrogen content

In agreement with previous studies [34,44,75], fuel hydrogen content is observed to correlate with nvPM emissions. Averages were calculated from data at 1.9-2.4 bar, as these were perceived as the most representative of real-life pressurised combustor systems. The use of the highest hydrogen content fuel (A-LA) resulted in average reductions in EI_{mass}, EI_{number} and combustor-exit GMD compared to J-REF of 73%, 54% and 17%, respectively. Values of EI_{number} corrected for thermophoresis but not size dependant system losses, exhibit a reduction of 60% for A-LA compared to J-REF, and therefore overreport percentage reductions by approximately 6%. A positive correlation between combustor pressure and combustor-exit nvPM EI_{mass}, EI_{number} and GMD is also observed. Scatter surrounding the hydrogen content trendlines is believed to be indicative of combustor rig variability, further supported by the correlating gaseous emissions Figure 11. For example, J-HA was observed to produce the highest nvPM emissions which was unexpected given it had a hydrogen content $0.139\%_{mass}$ lower than fuel A-HA. The corresponding gaseous data shows that NOx emissions produced by this fuel were comparably lower, while CO and UHC emissions were higher. This is indicative of a lower flame temperature and less efficient, richer combustion, which is also supported by a lower measured exhaust temperature. It was hypothesised that variations in specific fuel properties (e.g., fuel viscosity and surface tension) affecting atomisation may have contributed to this, however no correlation greater than the perceived measurement uncertainty and combustor repeatability was reliably established between individual properties and nvPM emissions.

The trendlines in **Figure 6** highlight the benefits of alternative fuels in affording reductions in nvPM mass, number and size compared to Jet A1 fuels. To quantify these reductions, combustor-exit nvPM EI_{number}, EI_{mass} and GMD were normalised to J-REF for all conditions (A-E) at the elevated 1.9 and 2.4 bara pressure cases, which are perceived as most representative of real-life pressurised combustor systems, with the data presented in **Figure 7** for combustor-exit nvPM (a), EI_{mass} (b) EI_{number} and (c) GMD. Again, only the 1.9 bar and 2.4 bar combustor pressure data were used for deriving the correlation, and it also noted that normalised value trends appeared to converge at these relatively higher pressures compared to lower pressures where higher scatter was observed, as exhibited in the trendline R^2 values. Second order polynomial hydrogen content fits have previously shown good correlations with nvPM

EI values [34,44], but modified inverse power fits are provided here as they better describe the potential physical reductions permissible, whilst also affording slightly higher R^2 values. The developed correlations ensured the fit would pass through the origin when hydrogen content was equal to that of J-REF, and that normalised nvPM values would tend towards a 100% reduction (zero nvPM) at the highest hydrogen contents. Using these trends, R^2 values of 0.816, 0.805 and 0.859 were obtained for loss corrected EI_{mass}, EI_{number} and GMD normalised to J-REF.

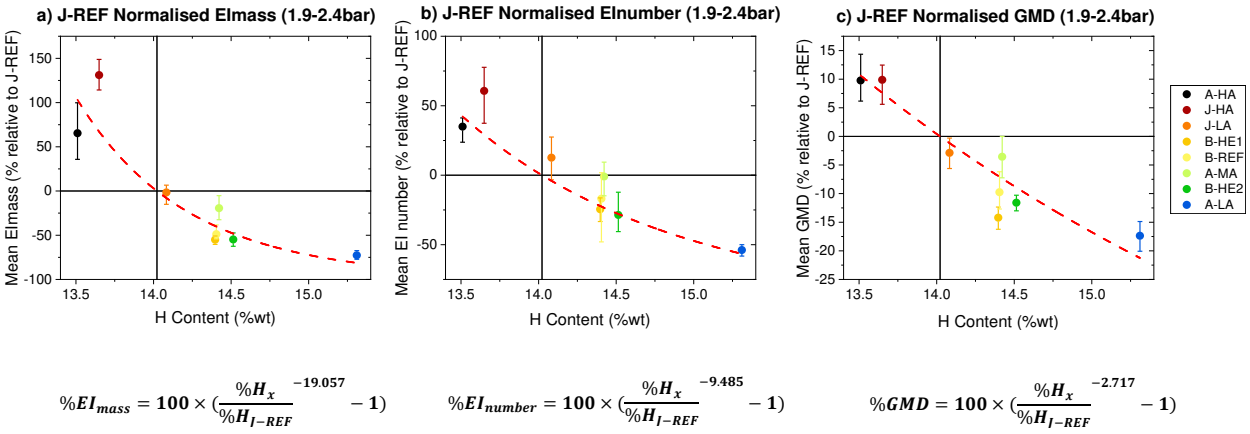

Figure 7: Combustor exit corrected nvPM data at 1.9bar and 2.4bar both at condition C normalised to J-REF for EI_{mass} (a), EI_{number} (b), and GMD (c) with derived hydrogen content trendlines (weightings turned off)

4.1.2. Effect of RQL Combustor Operating Conditions on nvPM emissions

The impact of fuel flow rate, primary air and secondary air on nvPM emissions was assessed by varying one parameter while keeping the others constant, with results shown at a representative condition (J-REF fuel at 1.9 bar combustor pressure) in **Figure 8, Figure 9 and Figure 10.** Increasing fuel flowrate from 1.4 to 1.6 g/s was seen to reduce nvPM EI_{number} and EI_{mass} at rates similar to each other, while having no observable effect on GMD (**Figure 8**). An increase in fuel flow rate by 0.2 g/s increased the global equivalence ratio from 0.31 to 0.35 and the primary equivalence ratio from 2.9 to 3.3 (including cooling air). The higher fuel flowrate was accompanied by an increase in the measured combustor exhaust temperatures (~+60K from 1.4g/s to 1.6g/s), subsequently leading to an increase in NOx

emissions (see Appendix). The increased heat release appears to result in higher nvPM oxidation rates resulting in fewer particles of similar average size per kg fuel burned [8].

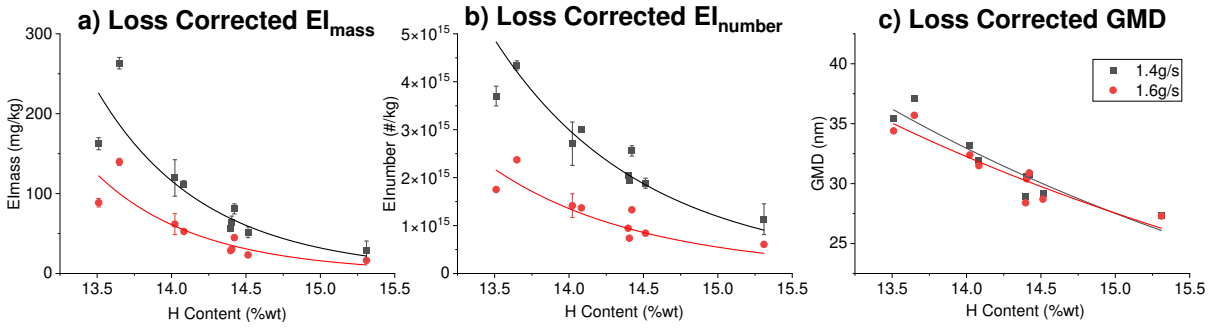

Figure 8: Effect of varying the fuel flow rate (Condition B to D) on combustor-exit nvPM EI_{mass} (a) EI_{number} (b) and GMD (c)

Increasing the primary air flowrate from 4.2 to 4.8 g/s was observed to reduce the nvPM EI_{mass} and GMD but had little observable impact on nvPM EI_{number} (**Figure 9**), suggesting it mostly resulted in partial oxidation of the larger particles (i.e., the right tail of the particle size distribution). Increasing primary air would be expected to affect combustion by improving atomisation quality due to the higher relative velocity between air and fuel. Using **equation (1)**, SMDs were predicted to decrease by 9-13µm (~20-30% reduction) between these conditions for all fuels. The increase in primary air also lowered the primary equivalence ratio from 3.7 to 3.3. Both of these changes could be expected to reduce nvPM emissions. The increase in atomiser exit airspeed may also have decreased the residence time of the flame in the combustor, which would be expected to reduce soot oxidation [3].

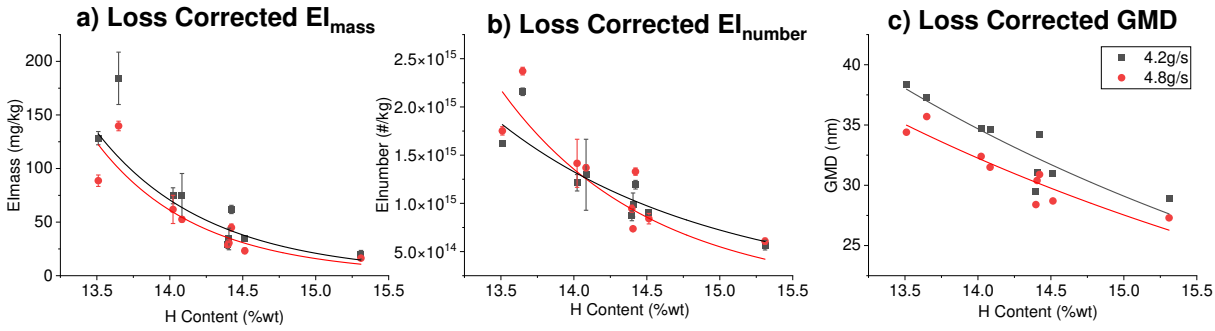

Figure 9: Effect of varying the primary air (Condition C to D) on combustor-exit nvPM EI_{mass}, (a) EI_{number}(b) and GMD (c)

Increasing the secondary air flowrate from 60 to 70 g/s was observed to increase nvPM EI_{number} and mass but decrease the GMD, which can be explained by the fact that the relative increase in nvPM EI_{number} was higher than the increase in nvPM EI_{mass} (**Figure 10**). Increasing the secondary air flowrate lowered the global equivalence ratio from 0.35 to 0.31 and slightly reduced the primary equivalence ratio from 3.3 to 3.2 due to an increase in air entering via the primary cooling holes. This may have promoted air impingement and soot "freezing", where the rapid decrease in temperature at the surface of nvPM particles resulted in decreased soot oxidation [8]. This allows more smaller particles to propagate through the combustor, thereby increasing particle number while reducing the overall GMD and increasing the right tail of the particle size distribution.

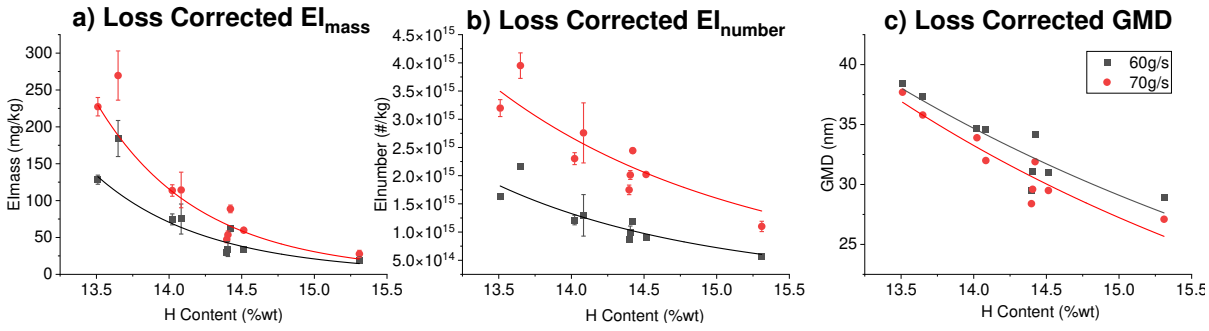

Figure 10: Effect of varying the secondary air (Condition C to E) on combustor-exit nvPM EI_{mass} (a), EI_{number} and (b) GMD (c)

From the above observations, it can be concluded that the availability of more air, whether introduced through the atomiser or combustor liner, results in smaller average particle size, but this does not correlate directly to either primary or global equivalence ratio since increasing fuel flow had little effect on GMD. EI_{number} however correlated well with both global equivalence ratio and combustor temperature, where a global equivalence ratio closer to stoichiometry and higher combustion temperature resulted in fewer particles of a similar average size. Furthermore, increasing secondary air generally worsened overall nvPM emissions, suggesting higher incidences of soot "freezing".

4.2. Gaseous Emissions

The raw gaseous CO_2, EI_{CO}, EI_{NOx} and EI_{UHC} emissions for all fuels investigated at different combustor pressures are presented in **Figure 11** at the condition C representative of other investigated conditions, with the complete gaseous dataset available in the Appendix. Error bars are representative of ±2 standard deviations, and show high stability for all gaseous measurements.

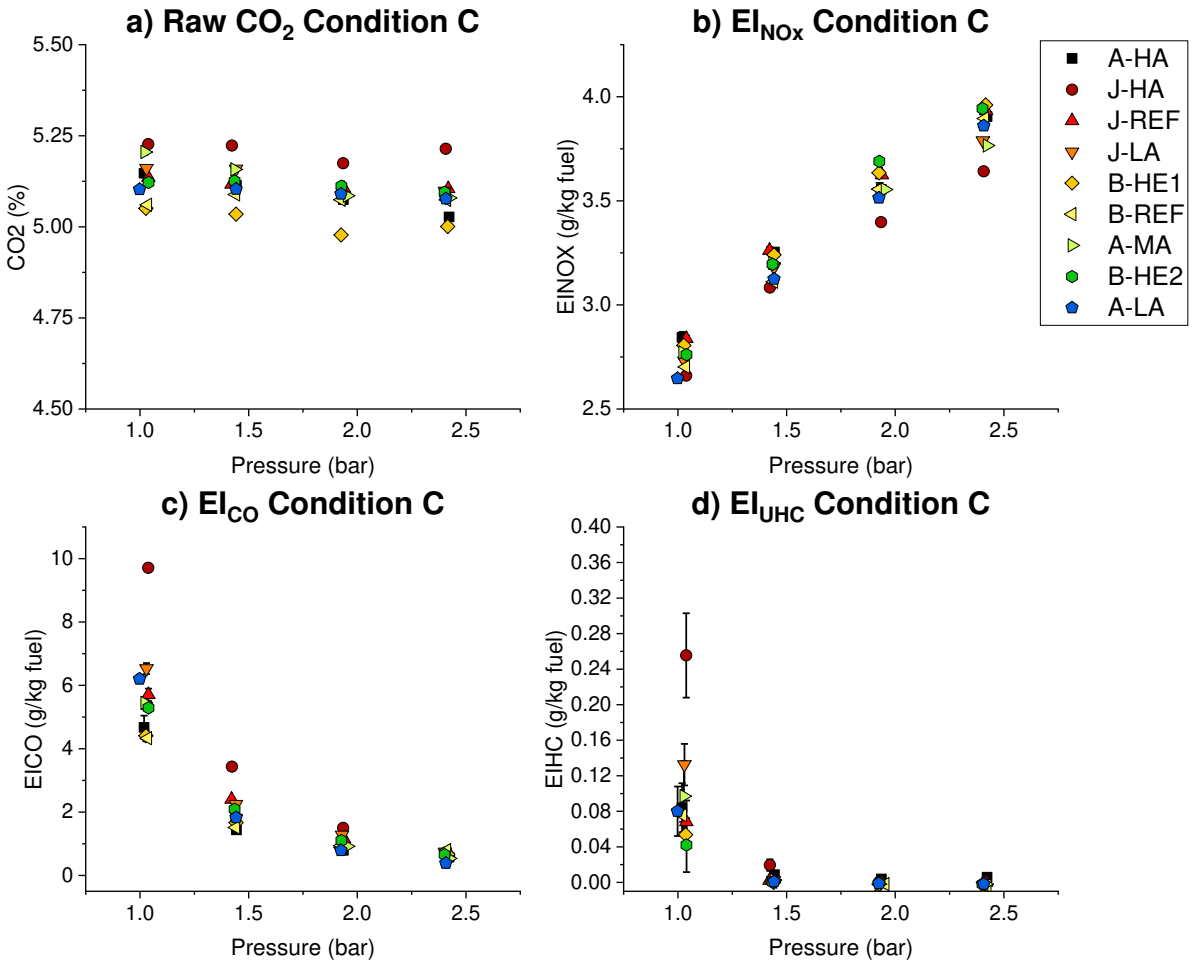

Figure 11: Raw CO_2 (a), EI_{NOx} (b), EI_{CO} (c) and EI_{UHC} (d) for the nine investigated fuels at different combustor pressure and RQL rig condition C

The raw CO_2 emissions ranged from 4.98% to 5.23% at condition C (**Figure 11 (a)**), with an average of 5.32% ±2.42%. This agrees with the estimated measurement uncertainty for gaseous measurements of ±2.69% [67]. Fuel J-HA is seen to consistently exhibit higher CO_2 emissions, while fuel B-HE1 produced relatively lower CO_2 emissions when compared with other investigated fuels. These deviations are most likely due to the aforementioned gas analyser uncertainties, but may also have been

a result of deviations in actual test point AFR, either due to uncertainties associated with the mass flow controllers used to control fuel and air flow. AFR values calculated using the SAE gas analysis tool are included in the appendix. EI_{CO} and EI_{UHC} emissions were low across testing and very stable, with the highest values observed at the 1.0 bar combustor pressure. This is indicative of poorer combustion efficiency, a result of worsened atomisation and relatively lower thermal power. Overall combustion efficiencies calculated using the SAE gas analysis tool are also included in the appendix, and show deteriorating values at 1 bar pressure conditions as low as 99.26% (J-HA). As pressure and primary air flowrates increase, EI_{CO} and EI_{UHC} drop by an order of magnitude to the limit of detection for all fuels between 1.0 and 2.4 bar, with calculated combustion efficiencies above 99.8% for all conditions ≥1.4 bar.

5. Conclusions

A full dataset of corrected aviation regulatory compliant nvPM and gaseous emissions is provided for nine fuels (three conventional aviation fuels, three SAF fuels, and three blends) within a non-proprietary scaled RQL combustion rig. The RQL combustor was operated at different pressures and AFRs producing a range of nvPM emissions similar to those observed with modern gas turbine engines. The nvPM emissions were measured using the European nvPM reference system and were corrected for sampling and measurement system particle loss using additional particle size measurement to provide values representative of the combustor-exit and facilitate future modelling studies in the study of alternative fuel properties on nvPM emissions.

Combustor-exit nvPM EI_{mass}, EI_{number} and GMD were all shown to correlate with the fuel hydrogen content trend. Average emission reductions of 73%, 54% and 17% for particle mass, number, and size respectively, were achieved by the use of a near-zero aromatic ATJ fuel compared to a reference Jet A1 fuel (14.022% hydrogen content). Reductions in EI from increasing fuel hydrogen content were shown to be overpredicted when uncorrected for line losses. The influence of fuel flowrate, primary air and secondary air on emissions was examined. Increasing combustor pressure was found generally to exacerbate both combustor-exit nvPM EI_{number}, mass and GMD. Increasing fuel flowrate reduced

combustor-exit nvPM EI_{number} but had little impact on particle sizes. Increasing primary air was found to reduce combustor-exit nvPM EI_{mass} through decreases in particle sizes but had little impact on nvPM EI_{number}. The results appear to indicate that increases in combustor temperature and global equivalence ratio correlate best to EI_{number}, while the availability of air either through the atomiser or combustion liner correlate inversely with GMD.

The results of this study provide a unique and novel dataset of nvPM and gaseous emissions from a non-proprietary RQL combustor, with detailed geometry and operating parameters provided, suitable for development and validation of modelling studies, required to investigate the impact of alternative fuel properties and combustor operating conditions on nvPM emissions in current and future combustor technologies. The full experimentation dataset (raw measured and processed/corrected) acquired during the test campaign is available in the appendix along with full CAD files of the combustor rig.

6. Acknowledgements

Funding: The experimental programme of work received funding from the European Union's Horizon 2020 research and innovation JETSCREEN programme under grant agreement No 723525 with support from Clean Sky 2 Joint undertaking under the European Union's Horizon 2020 research and innovation RAPTOR programme (Grant agreement ID: 863969)] used to prepare this publication.

The authors would also like to acknowledge EASA for the loan of the EUR nvPM mobile reference system under contract EASA. 2015.C01.AM01.

Special thanks also go to Dr Bastian Rauch of the German Aerospace Centre (Deutsches Zentrum für Luft und Raumfahrt) Institute of Combustion Technology for facilitating a detailed fuel analysis of the reported fuels, GTRC staff members Steve Morris, Jack Thomas, and Anthony Giles for operating the Gas Turbine research facility and finally Dr Alison Paul and Craig James (Cardiff University School of Chemistry) for assessing the physical properties of the tested fuels.

7. References

[1] EASA. European Aviation Environmental Report 2019. 2019.
[2] Lobo P, Durdina L, Smallwood GJ, Rindlisbacher T, Siegerist F, Black EA, et al. Measurement

of Aircraft Engine Non-Volatile PM Emissions: Results of the Aviation-Particle Regulatory Instrumentation Demonstration Experiment (A-PRIDE) 4 Campaign. Aerosol Sci Technol 2015;49:472–84. https://doi.org/10.1080/02786826.2015.1047012.
[3] Durdina L, Brem BT, Abegglen M, Lobo P, Rindlisbacher T, Thomson KA, et al. Determination of PM mass emissions from an aircraft turbine engine using particle effective density 2014. https://doi.org/10.1016/j.atmosenv.2014.10.018.
[4] Boies AM, Stettler MEJ, Swanson JJ, Johnson TJ, Olfert JS, Johnson M, et al. Particle Emission Characteristics of a Gas Turbine with a Double Annular Combustor. Aerosol Sci Technol 2015;49:842–55. https://doi.org/10.1080/02786826.2015.1078452.
[5] Delhaye D, Ouf FX, Ferry D, Ortega IK, Penanhoat O, Peillon S, et al. The MERMOSE project: Characterization of particulate matter emissions of a commercial aircraft engine. J Aerosol Sci 2017;105:48–63. https://doi.org/10.1016/j.jaerosci.2016.11.018.
[6] Lobo P, Hagen DE, Whitefield PD, Raper D. PM emissions measurements of in-service commercial aircraft engines during the Delta-Atlanta Hartsfield Study. Atmos Environ 2015;104:237–45. https://doi.org/10.1016/j.atmosenv.2015.01.020.
[7] Williams A. Combustion of Liquid Fuel Sprays. 1st ed. Elsevier; 1990. https://doi.org/10.1016/C2013-0-00958-9.
[8] Lefebvre AH, Balal DR. Gas turbine combustion: alternative fuels and emissions. 3rd ed. CRC press; 2010.
[9] Masiol M, Harrison RM. Aircraft engine exhaust emissions and other airport-related contributions to ambient air pollution: A review. Atmos Environ 2014;95:409–55. https://doi.org/10.1016/j.atmosenv.2014.05.070.
[10] Jonsdottir HR, Delaval M, Leni Z, Keller A, Brem BT, Siegerist F, et al. Non-volatile particle emissions from aircraft turbine engines at ground-idle induce oxidative stress in bronchial cells. Commun Biol 2019;2:90. https://doi.org/10.1038/s42003-019-0332-7.
[11] World Health Organization. Health effects of particulate matter. 2013.
[12] Yim SHL, Lee GL, Lee IH, Allroggen F, Ashok A, Caiazzo F, et al. Global, regional and local health impacts of civil aviation emissions. Environ Res Lett 2015;10. https://doi.org/10.1088/1748-9326/10/3/034001.
[13] Kärcher B. The importance of contrail ice formation for mitigating the climate impact of aviation. J Geophys Res Atmos 2016;121:3497–505. https://doi.org/10.1002/2015JD024696.
[14] Burkhardt U, Bock L, Bier A. Mitigating the contrail cirrus climate impact by reducing aircraft soot number emissions. Npj Clim Atmos Sci 2018;1:37. https://doi.org/10.1038/s41612-018-0046-4.
[15] Lee DS, Fahey DW, Skowron A, Allen MR, Burkhardt U, Chen Q, et al. The contribution of global aviation to anthropogenic climate forcing for 2000 to 2018. Atmos Environ 2021;244. https://doi.org/10.1016/j.atmosenv.2020.117834.
[16] Kinsey JS, Hays MD, Dong Y, Williams DC, Logan R. Chemical Characterization of the Fine Particle Emissions from Commercial Aircraft Engines during the Aircraft Particle Emissions eXperiment (APEX) 1 to 3. Environ Sci Technol 2011;45:3415–21. https://doi.org/10.1021/es103880d.
[17] ICAO. Local Air Quality Technology Standards 2019. https://www.icao.int/environmental-protection/Pages/LAQ_TechnologyStandards.aspx (accessed July 31, 2021).
[18] ICAO. 2019 Environmental Report - The Next Chapter. 2019. https://doi.org/10.1089/hum.2015.29000.jmw.
[19] Liu Y, Sun X, Sethi V, Nalianda D, Li Y-G, Wang L. Review of modern low emissions combustion technologies for aero gas turbine engines. Prog Aerosp Sci 2017;94:12–45. https://doi.org/10.1016/j.paerosci.2017.08.001.
[20] ASTM. D1655-18 Standard Specification for Aviation Turbine Fuels. vol. i. 2018. https://doi.org/10.1520/D1655-10.2.
[21] Blakey S, Rye L, Wilson CW. Aviation gas turbine alternative fuels: A review. Proc Combust Inst 2011;33:2863–85. https://doi.org/10.1016/j.proci.2010.09.011.
[22] Frenklach M, Wang H. Detailed modeling of soot particle nucleation and growth. Symp Combust 1991;23:1559–66. https://doi.org/10.1016/S0082-0784(06)80426-1.
[23] Frenklach M. Reaction mechanism of soot formation in flames. Phys Chem Chem Phys

2002;4:2028–37. https://doi.org/10.1039/b110045a.
[24] Daggett D, Hadaller O, Hendricks R, Walther R. Alternative Fuels and Their Potential Impact on Aviation. CAS-Secretariat - 25th Congr. Int. Counc. Aeronaut. Sci., 2006, p. 2888–97.
[25] ICAO. Sustainable Aviation Fuels Guide. 2017. https://doi.org/10.1007/978-3-319-34181-1.
[26] Schmidt P, Batteiger V, Roth A, Weindorf W, Raksha T. Power-to-Liquids as Renewable Fuel Option for Aviation: A Review. Chemie Ing Tech 2018;90:127–40. https://doi.org/10.1002/cite.201700129.
[27] ASTM. D7566 − 20b Standard Specification for Aviation Turbine Fuel Containing Synthesized Hydrocarbons. 2020. https://doi.org/10.1520/D7566-20B.
[28] ICAO. Conversion processes 2021. https://www.icao.int/environmental-protection/GFAAF/Pages/Conversion-processes.aspx (accessed September 28, 2021).
[29] Corporan E, Edwards T, Shafer L, Dewitt MJ, Klingshirn C, Zabarnick S, et al. Chemical, thermal stability, seal swell, and emissions studies of alternative jet fuels. Energy and Fuels 2011;25:955–66. https://doi.org/10.1021/ef101520v.
[30] Corporan E, DeWitt MJ, Belovich V, Pawlik R, Lynch AC, Gord JR, et al. Emissions characteristics of a turbine engine and research combustor burning a Fischer-Tropsch jet fuel. Energy and Fuels 2007;21:2615–26. https://doi.org/10.1021/ef070015j.
[31] Anderson BE, Beyersdorf AJ, Hudgins CH, Plant J V, Thornhill KL, Winstead EL, et al. Alternative Aviation Fuel Experiment (AAFEX). 2011.
[32] Beyersdorf AJ, Timko MT, Ziemba LD, Bulzan D, Corporan E, Herndon SC, et al. Reductions in aircraft particulate emissions due to the use of Fischer–Tropsch fuels. Atmos Chem Phys 2014;14:11–23. https://doi.org/10.5194/acp-14-11-2014.
[33] Schripp T, Anderson B, Crosbie EC, Moore RH, Herrmann F, Oßwald P, et al. Impact of Alternative Jet Fuels on Engine Exhaust Composition During the 2015 ECLIF Ground-Based Measurements Campaign. Environ Sci Technol 2018;52:4969–78. https://doi.org/10.1021/acs.est.7b06244.
[34] Durand E, Lobo P, Crayford A, Sevcenco Y, Christie S. Impact of fuel hydrogen content on non-volatile particulate matter emitted from an aircraft auxiliary power unit measured with standardised reference systems. Fuel 2021;287. https://doi.org/10.1016/j.fuel.2020.119637.
[35] Lobo P, Rye L, Williams PI, Christie S, Uryga-Bugajska I, Wilson CW, et al. Impact of Alternative Fuels on Emissions Characteristics of a Gas Turbine Engine – Part 1: Gaseous and Particulate Matter Emissions. Environ Sci Technol 2012;46:10805–11. https://doi.org/10.1021/es301898u.
[36] Voigt C, Kleine J, Sauer D, Moore RH, Bräuer T, Le Clercq P, et al. Cleaner burning aviation fuels can reduce contrail cloudiness. Commun Earth Environ 2021;2. https://doi.org/10.1038/s43247-021-00174-y.
[37] Yang Y, Boehman AL, Santoro RJ. A study of jet fuel sooting tendency using the threshold sooting index (TSI) model. Combust Flame 2007;149:191–205. https://doi.org/10.1016/j.combustflame.2006.11.007.
[38] Kumal RR, Liu J, Gharpure A, Vander Wal RL, Kinsey JS, Giannelli B, et al. Impact of Biofuel Blends on Black Carbon Emissions from a Gas Turbine Engine. Energy & Fuels 2020;34:4958–66. https://doi.org/10.1021/acs.energyfuels.0c00094.
[39] Richter H, Howard J. Formation of polycyclic aromatic hydrocarbons and their growth to soot - a review of chemical reaction pathways. vol. 26. 2000. https://doi.org/10.1016/S0360-1285(00)00009-5.
[40] Reeves CM, Lefebvre AH. Fuel Effects on Aircraft Combustor Emissions. Proc. ASME 1986 Int. Gas Turbine Conf. Exhib. Vol. 3 Coal, Biomass Altern. Fuels; Combust. Fuels; Oil Gas Appl. Cycle Innov., American Society of Mechanical Engineers; 1986. https://doi.org/10.1115/86-gt-212.
[41] Botero ML, Mosbach S, Kraft M. Sooting tendency of paraffin components of diesel and gasoline in diffusion flames. Fuel 2014;126:8–15. https://doi.org/10.1016/j.fuel.2014.02.005.
[42] Zheng L, Ling C, Ubogu EA, Cronly J, Ahmed I, Zhang Y, et al. Effects of Alternative Fuel Properties on Particulate Matter Produced in a Gas Turbine Combustor. Energy & Fuels 2018;32:9883–97. https://doi.org/10.1021/acs.energyfuels.8b01442.
[43] Calcote HF, Manos DM. Effect of molecular structure on incipient soot formation. Combust

Flame 1983;49:289–304. https://doi.org/10.1016/0010-2180(83)90172-4.
[44] Lobo P, Christie S, Khandelwal B, Blakey SG, Raper DW. Evaluation of Non-volatile Particulate Matter Emission Characteristics of an Aircraft Auxiliary Power Unit with Varying Alternative Jet Fuel Blend Ratios. Energy & Fuels 2015;29:7705–11. https://doi.org/10.1021/acs.energyfuels.5b01758.
[45] Xue X, Hui X, Singh P, Sung CJ. Soot formation in non-premixed counterflow flames of conventional and alternative jet fuels. Fuel 2017;210:343–51. https://doi.org/10.1016/j.fuel.2017.08.079.
[46] Zhang C, Hui X, Lin Y, Sung C-J. Recent development in studies of alternative jet fuel combustion: Progress, challenges, and opportunities. Renew Sustain Energy Rev 2016;54:120–38. https://doi.org/10.1016/j.rser.2015.09.056.
[47] Zahmatkesh I, Moghiman M. Effect of liquid fuel droplet size on soot emission from turbulent spray flames. Iran J Sci Technol Trans B Eng 2006;30:339–51.
[48] Charalampous G, Hardalupas Y. How do liquid fuel physical properties affect liquid jet development in atomisers? Phys Fluids 2016;28. https://doi.org/10.1063/1.4965447.
[49] Di Domenico M, Gerlinger P, Aigner M. Development and validation of a new soot formation model for gas turbine combustor simulations. Combust Flame 2010;157:246–58. https://doi.org/10.1016/j.combustflame.2009.10.015.
[50] Sharma S, Singh P, Gupta A, Chowdhury A, Khandelwal B, Kumar S. Distributed combustion mode in a can-type gas turbine combustor – A numerical and experimental study. Appl Energy 2020;277. https://doi.org/10.1016/j.apenergy.2020.115573.
[51] Dooley S, Won SH, Chaos M, Heyne J, Ju Y, Dryer FL, et al. A jet fuel surrogate formulated by real fuel properties. Combust Flame 2010;157:2333–9. https://doi.org/10.1016/j.combustflame.2010.07.001.
[52] Mensch A, Santoro RJ, Litzinger TA, Lee SY. Sooting characteristics of surrogates for jet fuels. Combust Flame 2010;157:1097–105. https://doi.org/10.1016/j.combustflame.2010.02.008.
[53] Dagaut P. Kinetics of Jet Fuel Combustion Over Extended Conditions: Experimental and Modeling. J Eng Gas Turbines Power 2007;129:394. https://doi.org/10.1115/1.2364196.
[54] Colket M, Edwards T, Williams S, Cernansky NP, Miller DL, Egolfopoulos F, et al. Development of an experimental database and kinetic models for surrogate jet fuels. 45th AIAA Aerosp. Sci. Meet. Exhib., 2007, p. 1–21. https://doi.org/10.4271/2007-01-0201.
[55] Saggese C, Ferrario S, Camacho J, Cuoci A, Frassoldati A, Ranzi E, et al. Kinetic modeling of particle size distribution of soot in a premixed burner-stabilized stagnation ethylene flame. Combust Flame 2015;162:3356–69. https://doi.org/10.1016/j.combustflame.2015.06.002.
[56] Wang H, Xu R, Wang K, Bowman CT, Hanson RK, Davidson DF, et al. A physics-based approach to modeling real-fuel combustion chemistry - I. Evidence from experiments, and thermodynamic, chemical kinetic and statistical considerations. Combust Flame 2018;193:502–19. https://doi.org/10.1016/j.combustflame.2018.03.019.
[57] Stöhr M, Geigle KP, Hadef R, Boxx I, Carter CD, Grader M, et al. Time-resolved study of transient soot formation in an aero-engine model combustor at elevated pressure. Proc Combust Inst 2019;37:5421–8. https://doi.org/10.1016/j.proci.2018.05.122.
[58] Xu R, Wang K, Banerjee S, Shao J, Parise T, Zhu Y, et al. A physics-based approach to modeling real-fuel combustion chemistry – II. Reaction kinetic models of jet and rocket fuels. Combust Flame 2018;193:520–37. https://doi.org/10.1016/j.combustflame.2018.03.021.
[59] SAE Aerospace. Aerospace Recommended Practice ARP6481. 2019.
[60] ASTM. D7171-16 Standard Test Method for Hydrogen Content of Middle Distillate Petroleum Products by Low-Resolution Pulsed Nuclear Magnetic Resonance. 2016. https://doi.org/10.1520/D7171-05R11.2.
[61] MAKIDA M, YAMADA H, KUROSAWA Y, YAMAMOTO T, MATSUURA K, HAYASHI S. PRELIMINARY EXPERIMENTAL RESEARCH TO DEVELOP A COMBUSTOR FOR SMALL CLASS AIRCRAFT ENGINE UTILIZING PRIMARY RICH COMBUSTION APPROACH. ASME Turbo Expo 2006 2006:1–8.
[62] Simmons HC, Conrad RR, Orav M. AIR-ATOMIZING FUEL NOZZLE. 3,980,233, 1975.
[63] Crayford AP, Lacan F, Runyon J, Bowen PJ, Balwadkar S, Harper J, et al. Manufacture, Characterization and Stability Limits of an AM Prefilming Air-Blast Atomizer. Proc. ASME

Turbo Expo 2019 Turbomach. Tech. Conf. Expo. Vol. 4B Combust. Fuels, Emiss., Phoenix, Arizona, USA: American Society of Mechanical Engineers; 2019. https://doi.org/10.1115/GT2019-91624.
[64] Chin JS, Rizk NK, Razdan MK. Effect of Inner and Outer Airflow Characteristics on High Liquid Pressure Prefilming Airblast Atomization. J Propuls Power 2000;16:297–301. https://doi.org/10.2514/2.5568.
[65] Gupta AK, Lilley DG, Syred N, Gupta AK, Lilley DG, Syred N. Swirl flows. Abacus Press, Tunbridge Wells, Kent, England; 1984.
[66] Lobo P, Durdina L, Brem BT, Crayford AP, Johnson MP, Smallwood GJ, et al. Comparison of standardized sampling and measurement reference systems for aircraft engine non-volatile particulate matter emissions. J Aerosol Sci 2020;145. https://doi.org/10.1016/j.jaerosci.2020.105557.
[67] ICAO. Annex 16 - Environmental Protection. vol. 2. 2018.
[68] SAE Aerospace. ARP6320 Procedure for the Continuous Sampling and Measurement of Non-Volatile Particulate Matter Emissions from Aircraft Turbine Engines. 2017.
[69] SAE International. ARP1533C. 2016.
[70] Lefebvre AH, McDonell VG. Atomization and Sprays. 2nd ed. Boca Raton: CRC Press; 2017. https://doi.org/10.1201/9781315120911.
[71] El-Shanawany MS, Lefebvre AH. Airblast Atomization: The Effect of Linear Scale on Mean Drop Size. Proc. ASME Turbo Expo, vol. 1A-1980, American Society of Mechanical Engineers; 1980. https://doi.org/10.1115/80-GT-74.
[72] Tareq MM, Dafsari RA, Jung S, Lee J. Effect of the physical properties of liquid and ALR on the spray characteristics of a pre-filming airblast nozzle. Int J Multiph Flow 2020;126:103240. https://doi.org/10.1016/j.ijmultiphaseflow.2020.103240.
[73] Kinsey JS, Giannelli R, Howard R, Hoffman B, Frazee R, Aldridge M, et al. Assessment of a regulatory measurement system for the determination of the non-volatile particulate matter emissions from commercial aircraft engines. J Aerosol Sci 2021;154. https://doi.org/10.1016/j.jaerosci.2020.105734.
[74] Saffaripour M, Thomson KA, Smallwood GJ, Lobo P. A review on the morphological properties of non-volatile particulate matter emissions from aircraft turbine engines. J Aerosol Sci 2020;139:105467. https://doi.org/10.1016/j.jaerosci.2019.105467.
[75] Brem BT, Durdina L, Siegerist F, Beyerle P, Bruderer K, Rindlisbacher T, et al. Effects of Fuel Aromatic Content on Nonvolatile Particulate Emissions of an In-Production Aircraft Gas Turbine. Environ Sci Technol 2015;49:13149–57. https://doi.org/10.1021/acs.est.5b04167.